Similar but not the same: methods and applications of quantitative MRI to study muscular dystrophies

Veeger, T.T.J.

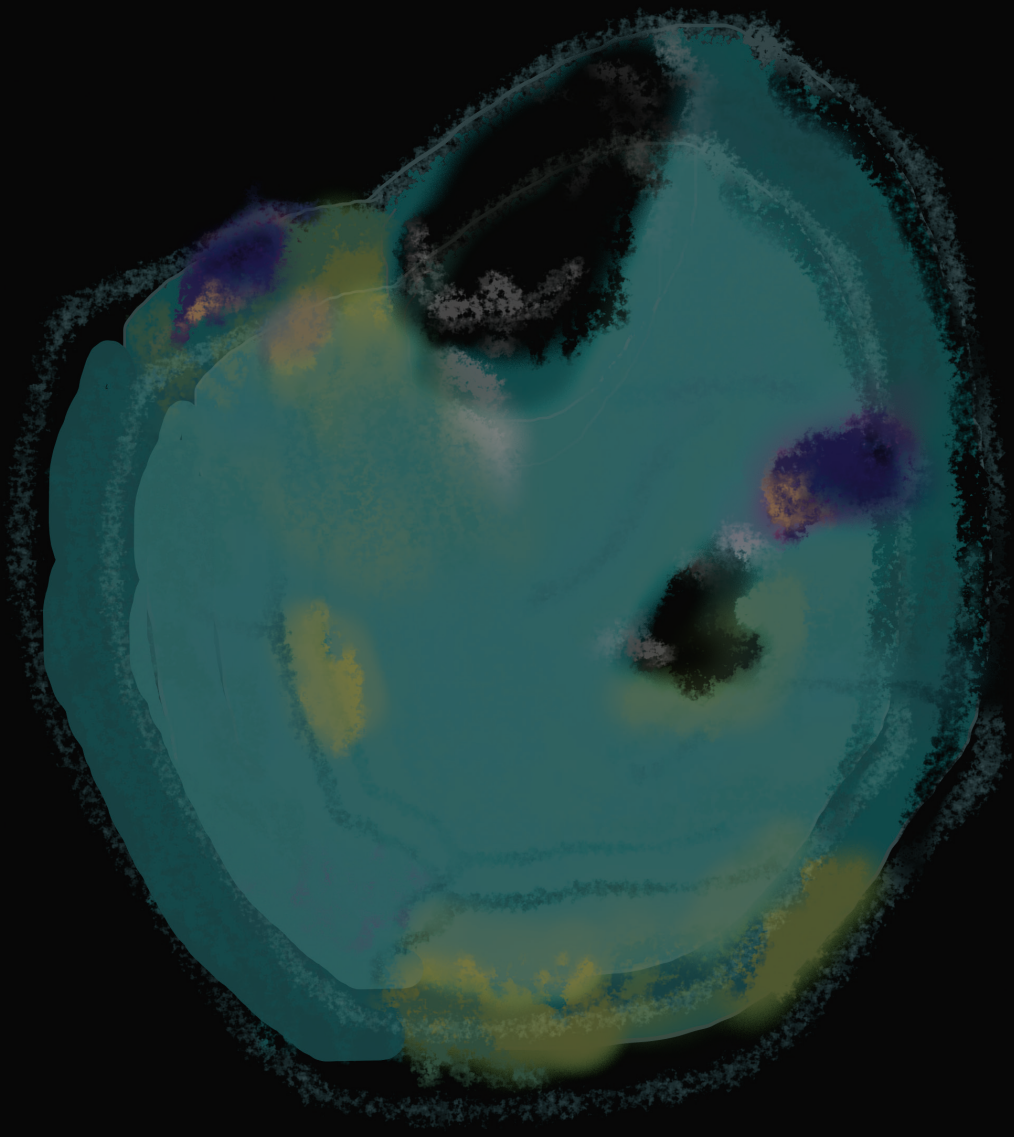

CHAPTER 5

SKELETAL MUSCLE STRAIN RATES DURING DYNAMIC CONTRACTIONS OF THE LOWER LEG ARE HETEROGENEOUSLY DISTRIBUTED

Melissa T. Hooijmans[1 *]
Thom TJ Veeger[2 *]
Valentina Mazzoli[3]
Hans C van Assen[4]
Jurriaan H de Groot[5]
Lukas M Gottwald[1]
Aart J Nederveen[1]
Gustav J Strijkers[6]
Hermien E Kan[2,7]

Submitted to NRM in Biomedicine

* Both authors contributed equally

1 Department of Radiology and Nuclear Medicine, Amsterdam University Medical Centers, University of Amsterdam, Amsterdam Movement Sciences, Amsterdam, The Netherlands
2 C.J. Gorter MRI Center, Department of Radiology, Leiden University Medical Center, Leiden, The Netherlands
3 Department of Radiology, Stanford University, Stanford, CA, USA
4 Department of Radiology, Leiden University Medical Center, Leiden, The Netherlands
5 Department of Rehabilitation Medicine, Leiden University Medical Center, Leiden, The Netherlands
6 Department of Biomedical Engineering and Physics, Amsterdam University Medical Centers, University of Amsterdam, Amsterdam Movement Sciences, Amsterdam, The Netherlands.
7 Duchenne Center Netherlands, The Netherlands

ABSTRACT

Background
Static quantitative MRI provides readouts of structural changes in diseased muscle but current approaches lack the ability to fully explain loss of contractile function. With Phase-Contrast MRI (PC-MRI), muscle contractile function can be assessed through quantification of strain rates. However, current 2D implementations are not sufficient to capture the complex motion of contracting muscle in the context of its 3D fiber architecture.

Purpose
To assess 3D strain rates along and perpendicular to the muscle fibers in lower leg muscles during dynamic exercise.

Study type
Observational

Population
12 healthy volunteers (age: 31.6 ± 15.9 years)

Field Strength/Sequence
3T, Chemical-shift-encoded water-fat separation scan, Spin Echo – Echo Planar Imaging with diffusion weighting and two time-resolved 3D PC-MRIs.

Assessments
PC-MRI acquisitions were done with and without load at 7.5% of the maximum voluntary dorsiflexion contraction force. Strain rates and diffusion tensors were calculated and combined to obtain strain rates along and perpendicular to the muscle fibers in seven lower leg muscles during dynamic dorsi-/plantarflexion movement cycle. To evaluate strain rates along the proximodistal muscle axis, muscles were divided into 5 equal segments.

Statistical tests
T-tests were used to test if cyclic strain rate patterns (amplitude >0) were present along and perpendicular to the muscle fibers. The effects of proximal-distal location and load were evaluated using repeated measures ANOVAs.

Results
Cyclic temporal strain rate patterns along and perpendicular to the fiber were found in all muscles involved in dorsi-/plantarflexion movement ($p<0.0017$). Strain rates along and perpendicular to the fiber were heterogeneously distributed over

the length of most muscles ($p<0.003$). Additional loading reduced strain rates of the extensor digitorum longus and gastrocnemius lateralis muscle ($p<0.001$).

Data conclusion

Lower leg muscles involved in cyclic dorsi-/plantarflexion exercise showed cyclic fiber strain rate patterns with amplitudes that varied between muscles and between the proximodistal segments within the majority of muscles.

INTRODUCTION

Quantitative Magnetic Resonance Imaging (MRI) is increasingly used to quantify healthy muscle architecture and architectural changes due to e.g. muscle disease, ageing, injury, and training interventions[1]. Muscle architectural features, including pennation angle, fiber length, and muscle volume are important determinants of muscle function[2-4], but also common compositional changes in disease, such as fibrosis and myosteatosis, influence muscle function[5,6]. Muscle composition and architecture can be assessed using a combination of quantitative MRI techniques including chemical shift based water-fat separation methods like the Dixon technique, T_2 or T_1 relaxometry, and Diffusion Tensor Imaging (DTI)[1]. However, static (qualitative and quantitative) MR readouts frequently fail to fully explain the loss of muscle function, particularly in neuromuscular diseases. For example, the gradual decrease in muscle strength characterizing various muscle diseases and sarcopenia cannot be solely explained by the loss in muscle volume[5-7]. This suggests that in these diseases there is a change in contractile function of the remaining muscle tissue that goes undetected using static MRI methods.

Muscle strain can provide a window on muscle contractile function, where strain is a local property of tissue that indicates the relative shortening or lengthening of tissue in a given direction. In skeletal muscle, strain rate (change in strain with respect to time) and strain have been examined using two-dimensional (2D) ultrasound and various MRI techniques[8-15]. 2D Ultrasound generates high spatial and temporal resolution images[16,17], but lacks the coverage and depth needed to assess full muscle strain distributions[18]. MRI has the ability to capture complete muscle volumes of multiple muscles simultaneously, but so far primarily focused on specific muscle parts or planes[8,11,19] using 2D implementations to reduce scan time. However, from studies in healthy muscle tissue, it is known that both architectural characteristics, i.e. pennation angle, and more functional features, i.e. microvascular function, vary between and within individual muscles[8,13,20-26], making such 2D implementations and focused studies incomplete. At the same time, this also indicates that it is generally impossible to define a MRI plane aligned with the muscle fibers, particularly during exercise when fibers are moving and deforming[8,27]. From strain measurements themselves it is not possible to infer the underlying fiber architecture, but combined with DTI strain can be calculated along and perpendicular to the muscle fibers. Additionally, the introduction of accelerated MRI facilitates 3D assessment of strain rate distributions with high temporal resolution (10ms) in full muscle volumes of the lower legs[27]. The combination of these techniques may create 3D strain distributions of full muscle volumes in relation with principal fiber directions to explore contractile function in skeletal muscle. This could be of specific interest for various muscle diseases and in sarcopenia where the lack of muscle function

cannot be fully explained by the loss in muscle volume. Hence, an advanced understanding of the role that contractile function may have in the decline in function in these population is essential with the prospect of developing strategies aimed at preserving and or improving muscle function.

Therefore, the main aim of this study was to assess whether 3D strain rate patterns can be measured along principal muscle fiber directions in the full volume of seven lower leg muscles during a cyclic dorsi-plantarflexion exercise, using an in-house developed accelerated time-resolved 3D PC-MRI protocol in combination with DTI. As a first application of this technology we investigated the (in)-homogeneity of muscle fiber strain rates along the proximodistal muscle axis of the leg muscles. Moreover, in order to assess strain rate in a condition more similar to a daily-life situation, we assessed whether the muscle fiber strain rates changed with an additional load. Based on the incompressibility phenomenon during muscle contraction[28], we hypothesize that muscles/muscle fibers of the lower leg involved in the dorsi-plantarflexion movement will shorten along the fiber during the contraction phase of the movement and concomitantly will expand perpendicular to the fiber. During the relaxation phase of the movement opposed behavior is expected, thereby introducing cyclic behavior. Based on the previously reported heterogeneously distributed architectural and functional features in skeletal muscle we hypothesize that strain rate amplitudes along and perpendicular to the fiber are also heterogeneously distributed along the proximodistal muscle axis. Lastly, with increasing load, a different execution of the dorsi-/plantarflexion movement is required and therefore differing strain rate amplitudes are expected in both the dorsi-flexor and plantar-flexor muscles compared to the unloaded condition.

MATERIALS AND METHODS

Participants

We collected data in the right lower leg of twelve healthy participants (age: 31.6±15.9 years; 50% m). The inclusion criteria were: no MRI contraindication, 18 years or older and no injuries or complaints of the lower extremity muscles. The study was approved by the institutional medical ethical committee according to the Medical Research Involving Human Subjects Act (WMO) and all participants provided written informed consent before participation.

Maximal Voluntary Contraction Force Measurements

First, the maximal voluntary isometric contraction force (MVCF) was assessed for the dorsi-flexor muscles using a handheld dynamometer (MicroFET2; Hoggan Scientific, Salt Lake City, Utah, USA). The participants were positioned in supine

position with an extended knee and the ankle in neutral position (0°). The dynamometer was placed on the forefoot, just distal to the toes, for each of the participants. The participants performed a maximal contraction against the dynamometer and repeated this three times. If the force kept increasing or if the difference between the measurements was more than 10%, up to two extra contractions were performed. The largest force recorded during these trials was considered to be the MVCF.

MR Data Acquisition

MR datasets were acquired in the right lower leg on a 3 Tesla MR System (Philips, Ingenia, Best, the Netherlands) using a 16-element receiver coil (anterior) and the 10-element receiver coil built into the patient table (posterior). The participants were positioned supine feet-first in the MR scanner with the right leg as close as possible to the center of the bore. The anterior coil was placed on top of the legs and supported with foam pillows and fixation bands to ensure that the coil covered the full lower leg and did not move during ankle dorsi-/planterflexion movement. The MR examination consisted of two parts with a total duration of 65 minutes, including repositioning in between the scans. The first part of the MR examination was performed with the ankle passively held in neutral angle (0°) to determine muscle fiber orientations and consisted of the following scans:

I Chemical shift-based water-fat separation scan (3D FFE; mDIXON quant (multi-echo); TR/TE/ΔTE/FA 7.8ms/1.27ms/1.1ms/3°; 6 echoes; voxel size 1x1x3mm^3; number of signal averages: 1; acquisition matrix: 192x192; number of slices 130; scan duration: 70.1 seconds) for muscle segmentation.

II Diffusion-weighted acquisition to assess principal fiber directions (Spin Echo – Echo Planar Imaging (SE-EPI); TR/TE: 6123ms/48ms; 24 directions; b-values: 0(5), 400(19) s/mm2; voxel size: 3x3x6mm3; number of signal averages: 1; acquisition matrix: 64x64; number of slices: 65; no slice gap, SENSE 1.9; combination of three fat suppression techniques: SPectral Adiabatic Inversion Recovery (SPAIR) and Slice Selected Gradient Reversal (SSGR) for the main aliphatic fat peak and a SPIR pulse for the olefinic fat peak; Partial Fourier factor: 0.73; scan duration: 290 seconds).

After changing the setup to facilitate the exercise task, the second part of the MR examination focused on retrieving velocity information during dynamic unconstrained dorsi-/plantarflexion movement, with the following scans:

I Chemical shift-based water-fat separation scan (3D FFE; mDIXON quant (multi-echo); TR/TE/ΔTE/FA 7.8ms/1.27ms/1.1ms/3°; 6 echoes; voxel size 1x1x3mm^3; number of signal averages: 1; acquisition matrix: 192x192; number

of slices 130; scan duration: 70.1 seconds) for muscle segmentation in neutral foot position.

II Two 4D PC-MRI acquisitions to retrieve velocity information during dorsi-/plantarflexion movement at 0.5 Hz (starting in plantarflexion), one with and one without load (FFE; TR/TE = 9.4/4.4 ms; VENC=10 cm/s; 3 velocity encoding directions; 20 time-steps, voxel size: 3x3x6mm^3; no fat suppression; scan duration of 432 seconds corresponding to 216 motion task repetitions) covering the full lower leg (FOV 192x192x390mm^3). The 216 motion task repetitions were needed in order to acquire the images of the 20 time-steps for the full FOV, resulting in one set of images representing one single movement cycle. The additionally applied load was 7.5% of the maximum voluntary contraction force (MVCF). 4D PC-MRI data were acquired by incoherently under-sampling k-space based on a pseudo-spiral pattern (under-sampling factor: R=9.1 with respect to a fully sampled data-set)[29].

The proximal end of the slice stack was positioned at the level of the tibia plateau and the midline of the imaging stack was aligned with the tibia bone for each of the MR sequences. A schematic representation of the exercise set-up is shown in Figure 1.

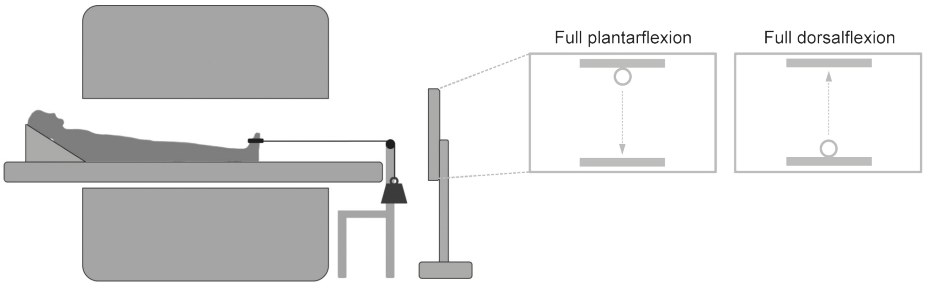

Figure 1. A schematic overview of the exercise set-up. The participants were positioned supine and were shown a screen for visual feedback of the motion task. The participants were asked to perform a dynamic dorsi- plantar flexion movement every 2 seconds, starting in plantar flexed position. For the load condition, a weight (7.5% of maximum voluntary contraction force) was attached to the ankle by a strap on the dorsal side of the foot.

Post-processing

All data were visually assessed for movement and fat artefacts. Chemical shift-based water-fat separation Dixon scans were reconstructed using scanner software. Diffusion datasets were processed using QMRITools (https://github.com/mfroeling/QMRITools) for Wolfram Mathematica 12. The diffusion data were de-noised using a principal-component analysis (PCA) algorithm and the diffusion-weighted images were spatially registered to b=0 images to correct

for motion and eddy current induced displacements using elastix (https://elastix.lumc.nl/; 26/08/2022)[30]. Thereafter, the diffusion data were registered to the Dixon water images, acquired just prior to the DTI acquisition, using a rigid registration and a B-spline registration to correct for EPI distortions. The diffusion tensor was calculated per voxel using an iterative Weighted-Linear-Least-Squares (iWLLS) algorithm. The tensor was diagonalized generating three eigenvectors (ev_1, ev_2, ev_3) per voxel. Signal-to-Noise-Ratios (SNR) were calculated per voxel based on the local average signal divided by the local noise sigma. DTI signal was determined on the b=0 image while the noise sigma was based on the background signal. Datasets with SNRs <20 were excluded from the analysis.

PC-MRI data were reconstructed using a Compressed Sensing pipeline[29] using BART. As a first step, the average velocity over all voxels and over the complete movement cycle was calculated and subtracted from the velocity data in order to exclude signal drift artefacts in the cyclic movement[9,27]. The resulting velocity data were then de-noised using a first order Gaussian filter (sigma = 1 voxel; through plane sigma 0.5 voxel) and used to calculate the 3D spatial gradient, the Jacobian (*J*) per voxel per frame (time).

$$J = \begin{bmatrix} \frac{\partial v_x}{\partial x} & \frac{\partial v_x}{\partial y} & \frac{\partial v_x}{\partial z} \\ \frac{\partial v_y}{\partial x} & \frac{\partial v_y}{\partial y} & \frac{\partial v_z}{\partial z} \\ \frac{\partial v_x}{\partial x} & \frac{\partial v_y}{\partial y} & \frac{\partial v_z}{\partial z} \end{bmatrix} \quad \text{Eq. 1}$$

From J the infinitesimal strain rate tensor (S) per voxel per frame (time) was calculated.

$$S(t) = \frac{1}{2}(J(t) + J(t)^T) \quad \text{Eq. 2}$$

This resulted in 3D strain rate tensor maps and 3D muscle fiber eigenvector maps for the full lower leg with a spatial resolution of 3x3x6 mm^3 and a temporal resolution of 100 ms. These 3D maps were used as input for further data-analysis.

Data analysis

Volumes of interest (VOIs) were manually drawn using the scanner reconstructed water images of the two Dixon acquisitions in neutral foot position. VOIs were drawn inside the border of the muscles along the full length of seven lower leg muscles for the fiber orientation (on the first acquired Dixon acquisition) and the velocity (on the second acquired Dixon acquisition) datasets separately using ITK-

snap (www.itksnap.org; version 3.6.0; April 2017)[31]. Seven lower leg muscles were analyzed, i.e. the tibialis anterior (TA), tibialis posterior (TP), extensor digitorum longus (EDL), peroneus (PER), soleus (SOL), gastrocnemius medialis (GCM) and gastrocnemius lateralis (GCL) muscles (Figure 2). Additionally, the SOL and TA were subdivided into smaller VOIs to account for the different compartments of these muscles[8,32]. For the SOL muscle, a lateral anterior compartment (SOLla), a medial anterior compartment (SOLma), a lateral posterior compartment (SOLlp) and a medial posterior compartment (SOLmp) were defined (Figure 2). The TA was subdivided in two compartments in the middle section where the muscle is separated by the intramuscular tendon, the superficial (TAsup), and the deep (TAdeep) compartments. Distal and proximal to the muscle belly, without a visible intramuscular tendon, the TA was drawn as one compartment (TAends) (Figure 2). The VOIs for the full TA muscle and SOL muscle were generated by combining the VOIs for the individual compartments. The reconstructed water images used for VOI selection were subsequently registered to individual time-steps (20) of the PC-MRI data (magnitude images) using the built-in *imregdemons* function in Matlab (version: 2019a), and the deformation matrices resulting from the registration were used to deform the VOIs to all the individual PC time-steps. Finally, the full muscle volumes were divided into five equal segments based on the normalized muscle length (i.e. distal segment (0-20%) – segment 20-40% – segment 40-60% – segment 60-80% – proximal segment (80-100%)). Four muscle compartments were only represented in the three mids segments covering 20 – 80% of the muscle (Figure 2).

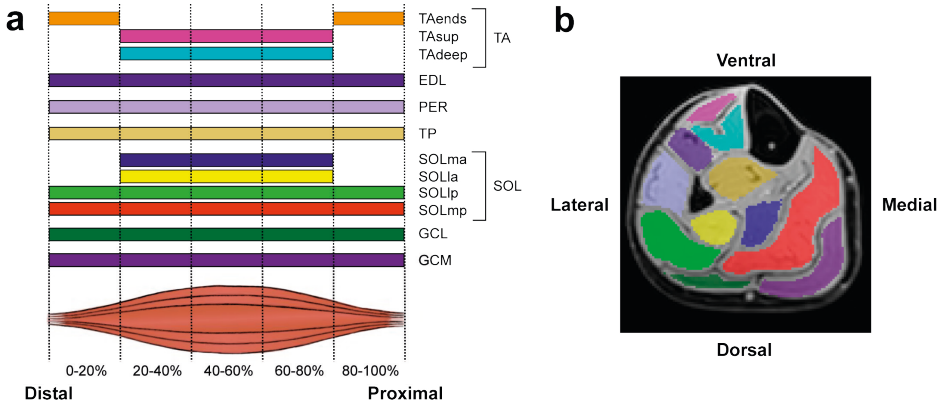

Figure 2. An overview of the manually segmented muscles and muscle compartments. Regions of interest for the individual muscles and muscle compartments (right-side) and their distribution along the length of the lower leg (left-side). TA: tibialis anterior; EDL: extensor digitorum longus; PER: peroneus; TP: tibialis posterior; SOLma: medial anterior compartment of the soleus muscle; SOLla: lateral anterior compartment of the soleus muscle; SOLlp: lateral posterior compartment of the soleus muscle; SOLmp: medial posterior compartment of the soleus muscle; GCL: lateral head of the gastrocnemius muscle; GCM: medial head of the gastrocnemius muscle.

To calculate strain rates along and perpendicular to the fiber our DTI and PC-MRI datasets had to be combined. Unfortunately, a voxel-by-voxel comparison was difficult due to differences in resolution and acquisition set-up. Therefore, first the most prominent fiber direction for every VOI was calculated as the weighted average principal eigenvector (ev_1) from the DTI (V_{along}) for every 10% section (s10%) of the total muscle length (Eq. 3). Due to the circular cross-sectional shape of the fiber the two perpendicular eigenvectors (ev_2 and ev_3) were interchangeable and dependent on the surroundings, and an average was not useful. Instead, the average principal fiber direction was used to define the cross-sectional plane of the fiber, by calculating vectors pointing in the two perpendicular directions in the plane perpendicular to V_{along}. (V_{p1} and V_{p2}; Eq. 4.1 and 4.2, respectively):

$$V_{along,s10\%} = \frac{\overline{ev_1}}{\|ev_1\|} \quad \text{Eq. 3}$$

$$V_{p1} = \frac{V_{along} \times [0 \quad 1 \quad 0]}{\left\| V_{along} \times [0 \quad 1 \quad 0] \right\|} \quad \text{Eq. 4.1}$$

$$V_{p2} = \frac{V_{along} \times V_{p1}}{\left\| V_{along} \times V_{p1} \right\|} \quad \text{Eq. 4.2}$$

These three unit vectors (V_{along}, V_{p1}, V_{p2}) were then used to calculate the strain rate in these directions (SR_{along}, SR_{p1}, SR_{p2}) on a voxel-by-voxel basis within all VOIs:

$$SR(t) = {V_{s10\%}}^T \cdot S(t) \cdot V_{s10\%} \quad \text{Eq. 5}$$

with t indicating every time point.

In order to get one strain rate measure resembling the expansion and compression in the perpendicular cross-sectional plane, with the same order of magnitude as the strain rate along the fiber, perpendicular cross-sectional area (CSA) strain rate (SR_{pCSA}) was calculated. First, SR_{p1} and SR_{p2} were used to calculate $\overline{SR_p}$, the average strain rate over the two directions (Eq. 5.1). $\overline{SR_p}$ was then used to calculate SR_{pCSA}, on a voxel-by-voxel basis using (Eq. 5.2 and 5.3):

$$\overline{SR_p}(t) = \frac{SR_{p1}(t) + SR_{p2}(t)}{2} \quad \text{Eq. 5.1}$$

$$\overline{SR_p}(t) > 0 : SR_{pCSA}(t) = \pi \cdot \overline{SR_p(t)}^2 \quad \text{Eq. 5.2}$$

$$\overline{SR_p}(t) < 0 : SR_{pCSA}(t) = -\pi \cdot \overline{SR_p(t)}^2 \quad \text{Eq. 5.3}$$

The negative π was used to maintain the sign of strain rate.

Weighted average and standard deviations were calculated for *SRalong* and SR_{pCSA} for all the five segmented VOIs from distal to proximal [0-20%; 20-40%; 40-60%; 60-80%, 80-100%] over time. This resulted in two strain rates, i.e. along the fiber direction, and in the plane perpendicular to the fiber direction.

Because of the cyclic nature of the exercise task, we modelled the resulting velocity time series to follow a sinusoidal pattern with a frequency of 0.5 Hz, i.e. one full cycle over two seconds. This cyclic trajectory is either starting with negative strain rates, or counterclockwise, starting with positive strain rates. Therefore, in order to enable comparison between time series a sinusoidal function with a frequency of 0.5 Hz was fitted to the data using a least squares method:

$$SR(t) = A \cdot sin(\pi t) + B \quad \text{Eq. 6}$$

with *A* the amplitude constrained between -5 and 5. Negative *A* indicates shortening/thinning and positive *A* indicates lengthening/thickening, and *B* the offset from zero.

Statistical analysis

Statistical analyses were performed using R (R Core Team, 2019) using the package *lme4* (Bates 2015). To assess the cyclic behavior for every muscle along and perpendicular to the fiber, one-sided t-tests were used to test if the average strain rate amplitudes (two amplitudes for every muscle/muscle compartment, along and perpendicular to the fiber) over all participants were significantly different from zero. The effect of load and proximal-distal location on strain rates along and perpendicular to the fiber for all muscles and compartments were assessed using multiple repeated measures ANOVAs, using a linear mixed model approach. These models included the strain rate amplitude (*A*) from the sinusoidal fits as outcome variable. The factors load condition (2 levels; load or no load) and proximodistal segment (5 levels) were added as independent predictors for strain rate amplitude *A*, including their interaction. Last, a by-participant random intercept was added to each model. For all tests the level of statistical significance was corrected for multiple testing (Bonferroni) and set at $p \leq 0.0018$ (i.e. 0.05/28 statistical tests, 14 muscle (-compartments) x 2 directions).

RESULTS

Study population & data quality

The dorsiflexion MVCF measured at the foot of our participants was 262.2± 57.7N and ranged between 185.5N and 411.5 N. None of the MRI datasets showed any motion or fat artefacts and all diffusion datasets were of sufficient SNR (>20) and thus included in the statistical analyses.

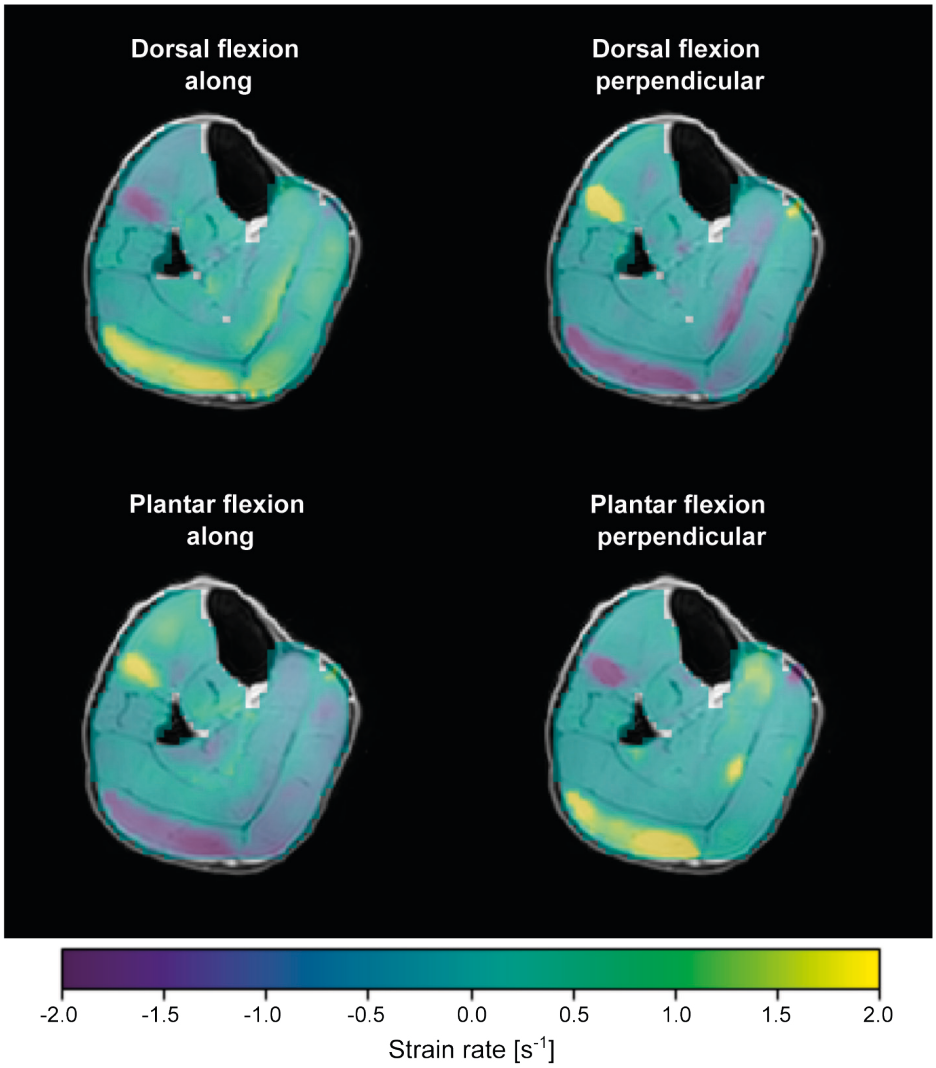

Figure 3. Example of cross-sectional images (Segment 40-60%segment) of the lower leg with color-coded strain rate amplitude along (left) and perpendicular (right) to the fiber during maximal dorsiflexion (top) and maximal plantarflexion (bottom) phase of the movement. Note the general antagonistic behavior in the anterior and posterior compartment of the lower leg. s = second

Temporal pattern of strain rates

Representative images color-coded for strain rate along and perpendicular to the fibers for one subject during maximal dorsiflexion velocity and maximal plantarflexion velocity without load are shown in Figure 3. In most lower leg muscles a significant cyclic temporal pattern, meaning an amplitude significantly different from zero, was found for strain rates along and perpendicular to the fiber ($p<.0018$), with varying amplitudes between muscles (Table 1).

Table 1. T-tests

		Along the fiber			Perpendicular to the fiber		
Muscles	**Compart-ments**	**Mean amplitude**	**CI**	**p-value**	**Mean amplitude**	**CI**	**p-value**
GCL		0.53	0.39 to 0.67	**<.0001**	-0.44	-0.57 to -0.30	**<.0001**
GCM		0.47	0.40 to 0.55	**<.0001**	-0.14	-0.19 to -0.10	**<.0001**
SOL		0.17	0.12 to 0.22	**<.0001**	-0.11	-0.14 to -0.08	**<.0001**
	SOLla	0.25	0.17 to 0.33	**<.0001**	-0.14	-0.21 to -0.07	**.0015**
	SOLma	0.20	0.11 to 0.28	**.0004**	-0.03	-0.07 to 0.02	.2119
	SOLlp	0.09	0.02 to 0.16	.0175	-0.04	-0.07 to -0.01	.0132
	SOLmp	0.20	0.14 to 0.26	**<.0001**	-0.17	-0.23 to -0.11	**<.0001**
EDL		-0.63	-0.80 to -0.45	**<.0001**	0.59	0.40 to 0.78	**<.0001**
TA		-0.31	-0.39 to -0.24	**<.0001**	0.13	0.08 tto 0.19	**.0003**
	TAdeep	-0.28	-0.40 to -0.17	**.0002**	0.16	0.06 to 0.26	.0053
	TAsup	-0.25	-0.36 to -014	**.0004**	0.16	0.06 to 0.27	.0066
	TAends	-0.41	-0.50 to -0.31	**<.0001**	0.08	0.04 to 0.12	**.0010**
PER		<0.01	-0.04 to 0.04	.8508	0.05	0.01 to 0.09	.0229
TP		0.01	-0.02 to 0.04	.5451	-0.01	-0.03 to 0.01	.1865

Amplitude estimates and p-values for the strain rates (s^{-1}) along and perpendicular to the fibers for the individual lower leg muscles and muscle compartments of the TA and SOL muscle. Significant differences, corrected for multiple testing, are indicated in bold ($p \leq 0.0018$). CI = 95% confidence interval; GCL = gastrocnemius lateralis; GCM = gastrocnemius medialis; SOL = soleus; SOLla = lateral anterior compartment of the soleus; SOLma = medial anterior compartment of the soleus; SOLlp = lateral posterior compartment of the soleus; SOLmp = medial posterior compartment of the soleus; EDL = extensor digitorum longus; TA = tibialis posterior; TAends = Two compartments distal and proximal of the tibialis anterior without visible intramuscular tendon; TAdeep = deep compartment of tibialis anterior; TAsup = superficial compartment of the tibialis anterior; PER = peroneus; TP = tibialis posterior.

For the GCM and GCL muscle, positive strain rates along the fiber related to ankle dorsiflexion, indicating lengthening of fibers, and negative strain rates perpendicular to the fibers, indicating thinning of fibers were seen (Figure 4).

During ankle plantarflexion, the opposite was observed with negative strain rates along (i.e. shortening) and positive strain rates perpendicular to (i.e. thickening) the muscle fiber (Figure 4). For the SOL muscle as a whole a cyclic pattern was observed but with smaller strain rate amplitudes along and perpendicular to the fibers in comparison with the GCM and GCL muscles during both the dorsi- and plantarflexion phase (Table 1 and red dashed lines in Figure 4). The individual compartments of the SOL muscle, however, showed more variability in strain rate amplitudes than the other plantar flexor muscles (Table 1 and red dashed lines in Figure 5). In the SOLal and SOLpm compartments significant cyclic patterns were measured along and perpendicular to the fiber, in the SOLam compartment only along the fiber, whereas in the SOLpl compartment a cyclic pattern in strain rate amplitudes, along and perpendicular to the muscle fibers, was absent ($p>.0018$).

In the antagonist TA and EDL muscles, an opposed cyclic pattern compared to the plantarflexion muscles was observed. This consisted of negative strain rate amplitudes along the fibers and positive strain rate amplitudes perpendicular to the fibers during ankle dorsiflexion, while this was opposite during plantarflexion (Table 1 and red dashed lines in Figures 6 and 7). The compartment analysis of the TA muscle was similar to the one of the full muscle. In the TP and PER muscles, cyclic patterns in strain rate amplitudes were absent both along and perpendicular to the muscle fibers ($p>.0018$) (Table 1 and Figure 7).

Proximodistal distribution of strain rates

The majority of the analyzed lower leg muscles showed a significant effect of proximodistal location on the strain rate amplitudes along the fibers (Table 2), except for the SOL muscle and SOL compartments. Strain rates perpendicular to the fibers were also heterogeneously distributed over the length of the muscle in the majority of muscles and muscle compartments except for the TP muscle and the TAends compartment (Table 2). The distribution of strain rate amplitudes along and perpendicular to the fibers was not consistent over all muscles. In general the absolute strain rate tended to increase either towards the proximal or distal muscle insertion. This resulted in the highest absolute strain rates in the 0-20% and 80-100% segment (i.e. TA, Figure 6) or the 20-40% and 60-80% segments (i.e. GCL, Figure 4). In the TAsup compartment, even opposite behavior between the most distal segment compared to the two other segments was seen, with negative amplitudes in the distal segment (20-40%) and positive amplitudes in the rest of the muscle segments (40-60% and 60-80%) (Figure 6).

Load effect

An effect of load on strain rate amplitudes along and perpendicular to the fiber was observed in the EDL and GCL (Table 1 & Supplemental material 1 - 4). In both muscles, lower strain rate amplitudes were measured in the loaded condition as compared to the condition without load ($p<.0001$; $p<.0001$)).

Table 2. Repeated Measures ANOVA results

			Along		Perpendicular	
Muscles	**Compartments**	**Effect**	**F-value**	**p-value**	**F-value**	**p-value**
GCL		Load	12.09	**.0007**	18.29	**<.0001**
		Segment	29.69	**<.0001**	38.10	**<.0001**
		Load x segment	0.66	.6227	1.54	.1945
GCM		Load	3.48	.0649	0.37	.5422
		Segment	10.88	**<.0001**	10.21	**<.0001**
		Load x segment	0.47	.7546	0.95	.4390
SOL		Load	1.29	2589	0.03	.8573
		Segment	1.14	.3397	9.14	**<.0001**
		Load x segment	0.30	.8741	0.58	.6752
	SOLla	Load	0.31	.5805	0.05	.8223
		Segment	2.91	.0625	1.64	.2026
		Load x segment	0.19	.8316	0.81	.4506
	SOLma	Load	3.02	.0875	0.57	.4552
		Segment	2.82	.0681	9.16	**.0003**
		Load x segment	0.64	.5327	0.27	.7644
	SOLlp	Load	0.88	.3491	0.58	.4474
		Segment	1.33	.2640	8.02	**<.0001**
		Load x segment	0.75	.5601	0.32	.8658
	SOLmp	Load	0.64	.4239	0.38	.5395
		Segment	4.44	.0023	10.23	**<.0001**
		Load x segment	0.19	.9408	0.77	.5446
EDL		Load	12.15	**.0007**	20.09	**<.0001**
		Segment	24.46	**<.0001**	19.92	**<.0001**
		Load x segment	0.65	.6257	1.64	.1703
TA		Load	1.00	.3184	0.53	.4667
		Segment	60.44	**<.0001**	8.17	**<.0001**
		Load x segment	0.37	.8305	0.01	.9998
	TAdeep	Load	<0.01	.9626	0.37	.5470
		Segment	25.80	**<.0001**	66.15	**<.0001**
		Load x segment	1.83	.1703	0.47	.6255
	TAsup	Load	0.23	.6326	0.07	.7965

Table 2. Continued.

			Along		Perpendicular	
Muscles	**Compartments**	**Effect**	**F-value**	**p-value**	**F-value**	**p-value**
		Segment	52.28	**<.0001**	16.12	**<.0001**
		Load x segment	0.08	.9210	0.12	.8841
	TAends	Load	0.05	.8253	1.87	.1814
		Segment	108.88	**<.0001**	2.25	.1429
		Load x segment	0.73	.3980	1.40	.2456
PER		Load	2.48	.1185	0.09	.7710
		Segment	20.35	**<.0001**	10.54	**<.0001**
		Load x segment	1.95	.1067	0.89	.4735
TP		Load	0.15	.6987	1.32	.2537
		Segment	5.08	**.0009**	0.89	.4700
		Load x segment	0.14	.9652	0.74	.5675

*F-values and p-values for the main effects of condition (no load ; loaded]), proximodistal location (for up to five segments of 20% muscle length, see Figure 2) and the interaction effect (load*segment) for strain rate Amplitudes along and perpendicular to the fibers during dorsi- and plantarflexion exercise for the individual muscles and muscle compartments are shown. Significant differences are indicated in bold (p≤0.0018). GCL = gastrocnemius lateralis; GCM = gastrocnemius medialis; SOL = soleus; SOLla = lateral anterior compartment of the soleus; SOLma = medial anterior compartment of the soleus; SOLlp = lateral posterior compartment of the soleus; SOLmp = medial posterior compartment of the soleus; EDL = extensor digitorum longus; TA = tibialis posterior; TAends = Two compartments distal and proximal of the tibialis anterior without visible intramuscular tendon; TAdeep = deep compartment of tibialis anterior; TAsup = superficial compartment of the tibialis anterior; PER = peroneus; TP = tibialis posterior.*

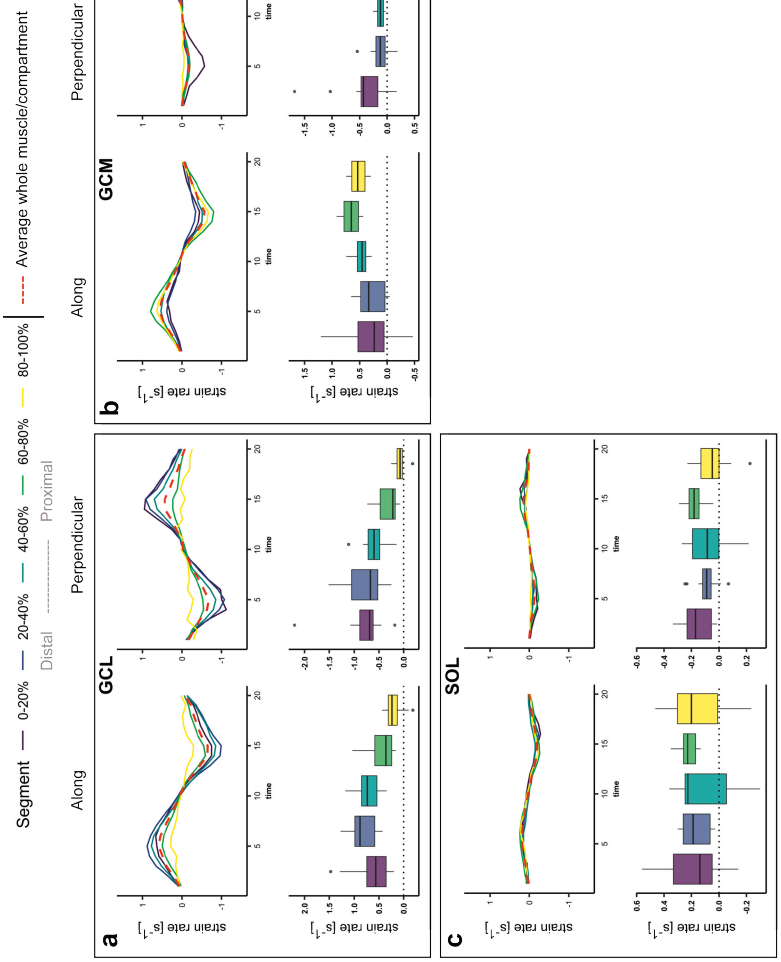

Figure 4. Line graphs with (top) strain rate along (left) and perpendicular (right) to the fibers in the GCL, GCM and SOL muscle during the full movement cycle for the exercise without load. The strain rate pattern in the full muscle volume is depicted with a red dotted line and the 5 individual segments are depicted in different colors (purple 0-20%; lila 20-40%; blue 40-60%; green: 60-80%; yellow 80-100%). Box plots are (bottom) strain rate amplitudes along (left) and perpendicular (right) to the fibers during maximum dorsi-flexion motion without load for the individual muscle segments, with colors matching the line graphs. To facilitate comparison between the absolute amplitudes along and perpendicular to the fibers, the y-axis of the graph showing strain rate along the fibers was inverted for the muscles expected to perform a dorsi-flexion movement. For the muscles expected to perform a plantarflexion movement, the y-axis of the graph of strain rate perpendicular to the fibers was inverted. GCL = gastrocnemius lateralis; GCM = gastrocnemius medialis; SOL = soleus.

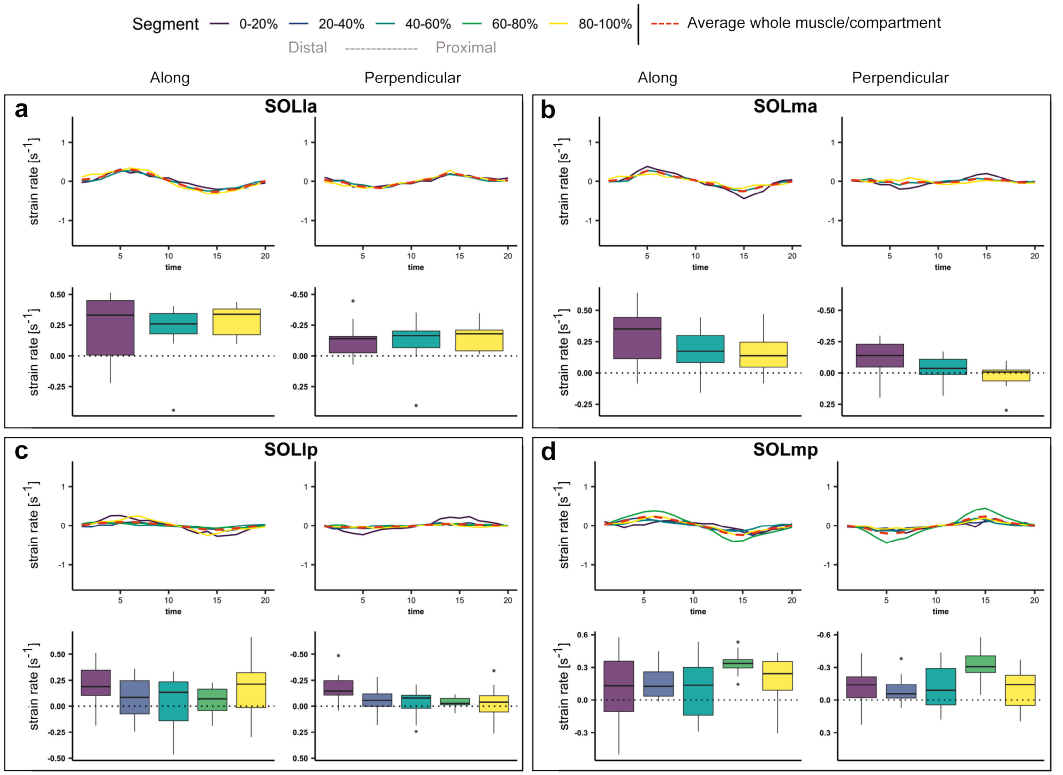

Figure 5. Line graphs with (top) strain rate along (left) and perpendicular (right) to the fibers in the four SOL compartments during the full movement cycle for the exercise without load. The strain rate pattern in the full muscle volume is depicted with a red dotted line and the 5 individual segments are depicted in different colors (purple 0-20%; lila 20-40%; blue 40-60%; green: 60-80%; yellow 80-100%). Box plots are (bottom) strain rates along (left) and perpendicular (right) to the fibers during maximum dorsi-flexion motion without load for the individual muscle segments, with colors matching the line graphs. Note the medial compartments of the soleus (SOLla and SOLma) are only present in the more distal part of the lower leg, see Figure 2. In order to facilitate the comparison between the absolute amplitudes along and perpendicular to the fibers, the y-axis of the graph with strain rate along the fibers was inverted for the muscles expected to perform a dorsi-flexion movement. For the muscles expected to perform a plantarflexion movement, the y-axis of the graph showing strain rate perpendicular to the fibers was inverted. SOL = soleus; SOLla = lateral anterior compartment of the soleus; SOLma = medial anterior compartment of the soleus; SOLlp = lateral posterior compartment of the soleus; SOLmp = medial posterior compartment of the soleus.

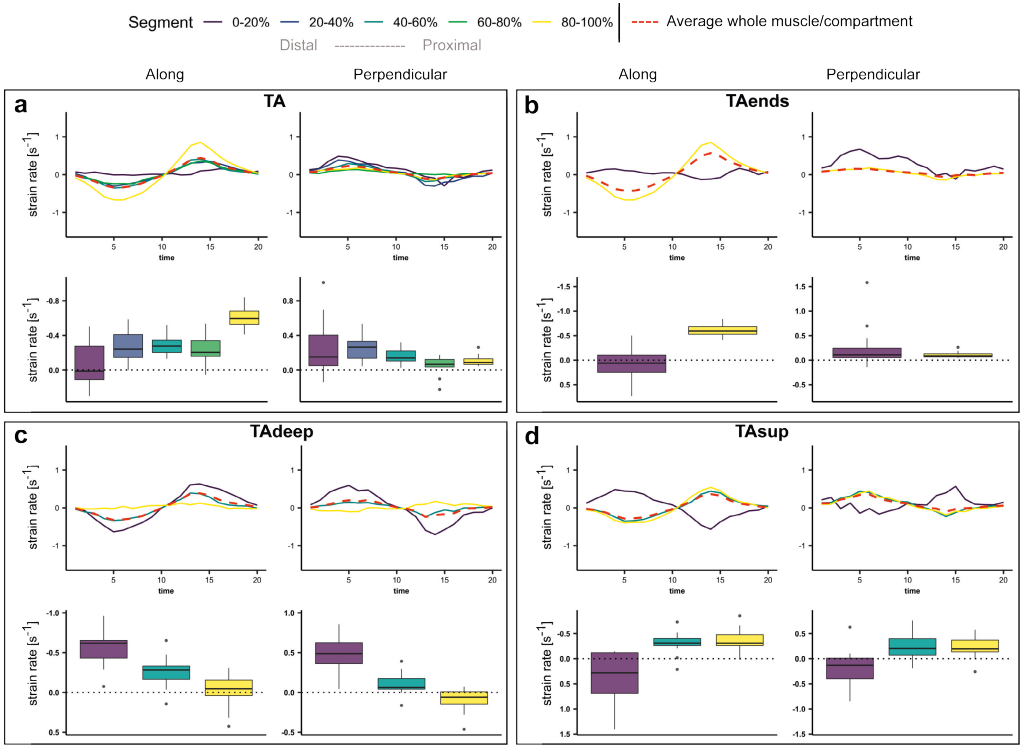

Figure 6. Line graphs (top) showing strain rate along (left) and perpendicular (right) to the fiber in the TA and the three TA compartments during the full movement cycle for the exercise without load. The strain rate pattern in the full muscle volume is depicted with a red dotted line and the 5 individual segments are depicted in different colors (purple 0-20%; lila 20-40%; blue 40-60%; green: 60-80%; yellow 80-100%). Box plots are (bottom) strain rates along (left) and perpendicular (right) to the fibers during maximum dorsi-flexion motion without load for the individual muscle segments, with colors matching the line graphs. Note not all compartments of TA muscle are continuously present along the proximodistal axis of the muscle, see Figure 2. To facilitate the comparison between the absolute amplitudes along and perpendicular to the fiber, the y-axis of the graph showing strain rate along the fibers was inverted for the muscles expected to perform a dorsi-flexion movement. For the muscles expected to perform a plantarflexion movement, the y-axis of the graph showing strain rate perpendicular to the fibers was inverted. TA = tibialis posterior; TAends = Two compartments distal and proximal of the tibialis anterior without visible intramuscular tendon; TAdeep = deep compartment of tibialis anterior; TAsup = superficial compartment of the tibialis anterior.

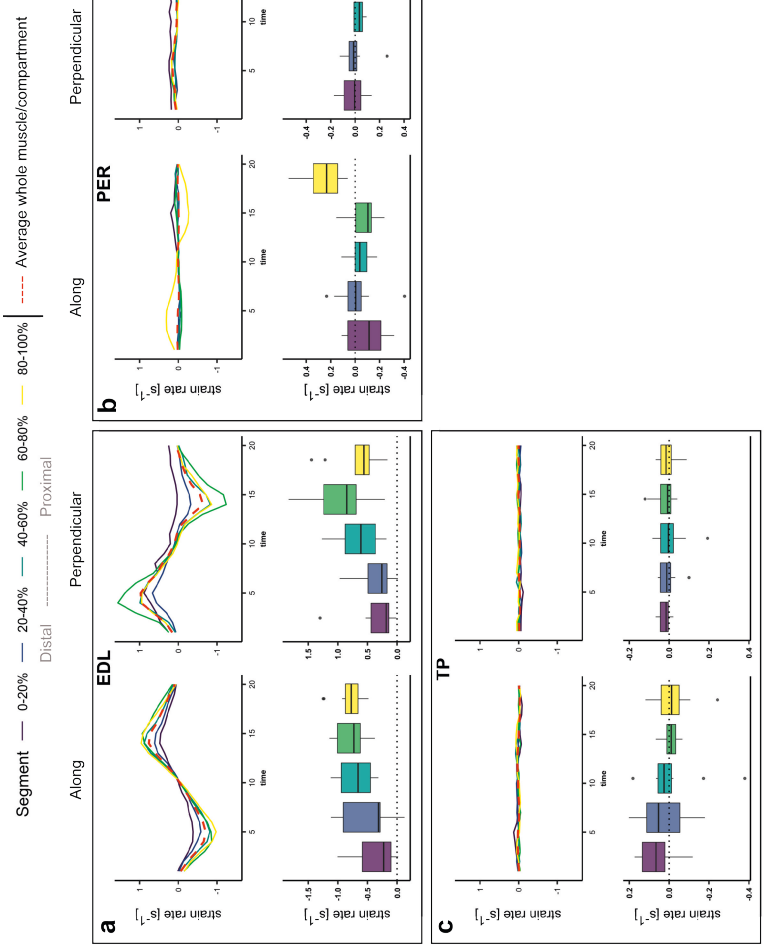

Figure 7. Line graphs (top) showing strain rate along (left) and perpendicular (right) to the fiber in the EDL, PER and TP muscle during the full movement cycle for the exercise without load. The strain rate pattern in the full muscle volume is depicted with a red dotted line and the 5 individual segments are depicted in different colors (purple 0-20%; lila 20-40%; blue 40-60%; green: 60-80%; yellow 80-100%). Box plots are (bottom) strain rates along (left) and perpendicular (right) to the fibers during maximum dorsi-flexion motion without load for the individual muscle segments, with colors matching the line graphs. In order to facilitate the comparison between the absolute amplitudes along and perpendicular to the fiber, the y-axis of the graph showing strain rate along the fiber was inverted for the muscles expected to perform a dorsi-flexion movement. For the muscles expected to perform a plantarflexion movement, the y-axis of the graph showing strain rate perpendicular to the fiber was inverted. EDL = extensor digitorum longus; PER = peroneus; TP = tibialis posterior.

DISCUSSION

This study demonstrates that it is feasible to assess strain rate along and perpendicular to muscle fibers covering the entire lower leg during dynamic dorsi-/plantarflexion exercise, using a combination of PC-MRI and DTI. The lower leg muscles and muscle compartments involved in repetitive dorsi-plantar flexion movements exhibited cyclic temporal patterns for strain rates along and perpendicular to the fibers for the full 3D muscle volumes. Furthermore, strain rates were heterogeneously distributed along the length of most of the lower leg muscles and muscle compartments. The strain rate amplitudes along and perpendicular to the fibers of the EDL and GCL muscle were smaller in the loaded condition.

In agreement with our first hypothesis, the temporal strain patterns in the primary plantarflexion muscles, i.e. the GCL, GCM, SOL (and compartments), started with lengthening along and thinning perpendicular to the fibers during the dorsi-plantarflexion movement. The primary dorsiflexion muscles of the ankle, the TA (and compartments) and EDL showed the expected opposite cyclic temporal strain rate patterns. The TP and PER muscles showed negligible average strain rate amplitudes along and perpendicular to the fibers. This is in line with their expected behavior during the dorsi-/plantarflexion movement as their primary function us to stabilize the ankle, rather than facilitate dorsi-/plantarflexion movement. The cyclic strain rate patterns observed in the plantar and dorsiflexor muscles, in combination with the absence of this pattern in the TP and PER muscles, demonstrates that the method is suitable to cover the full muscle volumes in 3D and during dynamic exercise.

Strain rate amplitudes along and perpendicular to the fibers were heterogeneously distributed over the proximodistal muscle axis in the majority of lower leg muscles, except for some of the SOL compartments and the TP muscle. The lower leg muscles with heterogeneous strain distributions primarily showed larger absolute strain rates in either the most distal or proximal segments, rather than the middle segments. A substantial number of previous studies investigated strain rate distributions in the lower leg muscles during passive lengthening and isometric contractions using 2D approaches, without correction for fiber orientations[8,13,19,21,25,26,33,34]. An inconsistent pattern was seen in these studies, where some reported homogeneous strain distributions over the muscle, and others described higher strain rates in distal parts of the muscle[13,25,26,33-36]. None of these studies combined strain measurements with DTI and therefore they could not express strain rates along and perpendicular to the muscle fibers, which makes a direct comparison with these previous works impossible. Nevertheless, the majority of mentioned factors linked to the strain heterogeneity in these

studies, for example fiber type distributions within the muscle, motor unit activation and neural control, are also valid for our results.

Interestingly, in the PER muscle we did not measure a cyclic pattern on a whole muscle basis, but on a more localized level a clear cyclic pattern with positive strain rate amplitudes along the fiber during dorsiflexion movement was observed in the most proximal segment. The PER muscle consists of three muscle heads, i.e. the peroneus longus, involved in plantarflexion and eversion of the ankle, the peroneus brevis, involved in plantarflexion and eversion of the ankle, and the peroneus tertius, involved in dorsiflexion and eversion of the ankle. These muscle heads are evaluated as one muscle although the origin and insertion of these heads are not equally distributed along the proximodistal muscle axis. The longus is primarily located in the most proximal muscle segments and our data suggest that there could be some selective involvement of this head during dynamic dorsi- and plantarflexion movement.

In addition to the observed heterogeneity in strain rates along the proximodistal axis, we also found variability in strain distributions in the different compartments of the SOL and TA muscles. The opposite cyclic temporal pattern in the distal segment of the TAsup compartment compared to the rest of the TA muscle suggesting lengthening and thinning of the muscle fibers during dorsiflexion of the ankle, was rather unexpected during this dorsi-plantar flexion movement. Currently, we do not have an explanation for this heterogeneity between compartments and segments. The fact that all muscles and compartments are interconnected via fascia and connective tissue could potentially result in intra- and inter-muscular force transmission which may underlie some of the displayed heterogeneity[37,38].

In the majority of lower leg muscles and compartments no effect of load was observed on the strain rate amplitudes along and perpendicular to the fiber. This could be due to the relatively small load we applied in the dorsiflexion direction, as other exercise studies primarily found that larger relative loads induced changes in measured strain and strain rate patterns[9,11,13,33,39]. In the GCL and EDL muscle, lower absolute strain rate amplitudes were observed along and perpendicular to the fiber during the loaded condition compared to the unloaded condition. For the GCL muscle, this may be related to how we applied load to the ankle. In our exercise set-up the load itself supported the plantarflexion movement of the ankle which may have resulted in a lower activity level in the GCL muscle.

The approach presented in this paper will facilitate in-depth studies on muscle 3D strain heterogeneity in relation to muscle architecture, composition,

and function, including properties such as fascicle lengths and curvature, (physiological) cross-sectional area, the extracellular matrix and fiber types within the muscle[8,40,41]. Furthermore, in combination with additional (imaging) techniques such as EMG, electrical stimulation and motor-unit MRI[42], more insights in motor unit activation and neural control in relation to muscle fiber strain and architecture can be obtained, which would help linking muscle contractile function to architecture and potentially to loss of function.

Our study has some limitations. First, we used the fiber orientation from the neutral (0°) ankle position to determine strain rate along and perpendicular to the fiber. During maximum dorsi- and plantarflexion and higher contraction intensities, pennation angles are known to be different compared to the neutral position[43]. This could have resulted in some under- or overestimation of longitudinal and transverse fiber strain rates reducing the sensitivity of the method for actual strain rate differences. However, a deviation of 20° in pennation angle would only cause an error of 6% strain rate (cosine (20°)), therefore it is unlikely that this explains the heterogeneity we found in strain rate amplitudes along and perpendicular to the fiber within the individual muscles, but also between individual muscles and compartments. Second, in order to acquire full volume strain rate values with a time resolution of 100 ms, 216 repetitions of the movement cycle were needed. This could have led to movement variance, despite the visual tracking cue, introducing some noise in the data. We do not expect that this affected the average strain rate patterns significantly as we observed consistent patterns over all participants, but it could be the cause for the small offset observed in some of the time series, most prominent in the condition with load. Given the cyclic nature of the movement, this offset is assumed to be false. Lastly, the loaded condition was always performed after the condition without load so there could be some fatigue effect influencing the repeatability of the movement in this condition which might has resulted in some additional noise in our findings.

In conclusion, this study shows that DTI and PC-MRI data can be combined to measure strain rate along and perpendicular to the fiber during dynamic exercise while covering the full lower leg. The muscles involved in the dorsi-/plantarflexion movement showed clear cyclic temporal strain rate patterns along and perpendicular to the fiber. Our data also revealed that the amplitudes of these cyclic strain rate patterns were significantly different along the proximodistal muscle axis of most muscles and compartments. In the future, this novel approach can be a valuable tool in studies aiming to link muscle function and muscle pathology.

STUDY FUNDING

This work was funded by the Dutch Technology Foundation TTW (DIMASK #15500), Amsterdam Movement Sciences grant and Netherlands Organization for Scientific Research (NWO), research program VIDI, project number 917.164.90.

SUPPLEMENTAL MATERIAL

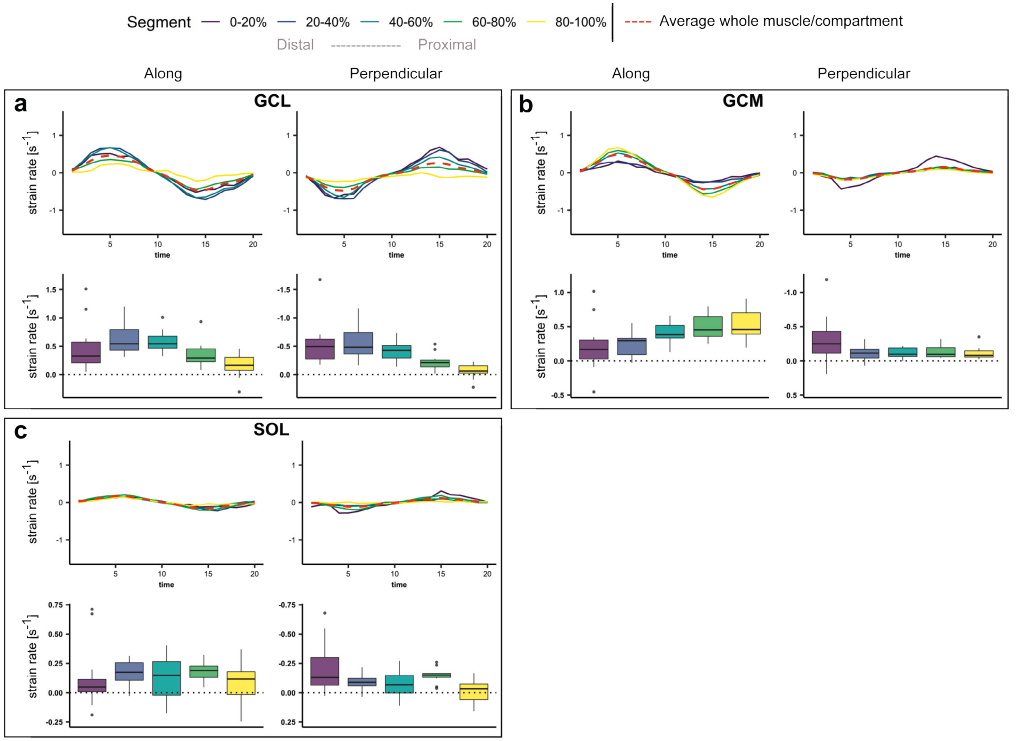

Supplemental figure 1. Line graphs with (top) strain rate along (left) and perpendicular (right) to the fibers in the GCL, GCM and SOL muscle during the full movement cycle for the exercise with load. The strain rate pattern in the full muscle volume is depicted with a red dotted line and the 5 individual segments are depicted in different colors (purple 0-20%; lila 20-40%; blue 40-60%; green: 60-80%; yellow 80-100%). Box plots are (bottom) strain rate amplitudes along (left) and perpendicular (right) to the fibers during maximum dorsi-flexion motion without load for the individual muscle segments, with colors matching the line graphs. To facilitate comparison between the absolute amplitudes along and perpendicular to the fibers, the y-axis of the graph showing strain rate along the fibers was inverted for the muscles expected to perform a dorsi-flexion movement. For the muscles expected to perform a plantarflexion movement, the y-axis of the graph of strain rate perpendicular to the fibers was inverted. GCL = gastrocnemius lateralis; GCM = gastrocnemius medialis; SOL = soleus.

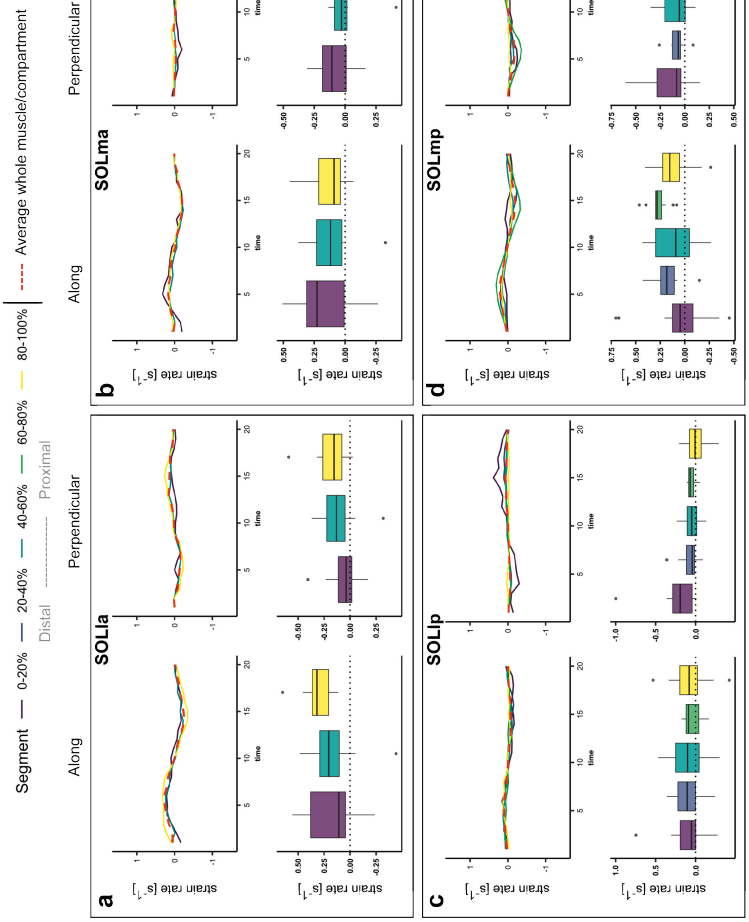

Supplemental figure 2. Line graphs with (top) strain rate along (left) and perpendicular (right) to the fibers in the four SOL compartments during the full movement cycle for the exercise with load. The strain rate pattern in the full muscle volume is depicted with a red dotted line and the 5 individual segments are depicted in different colors (purple 0-20%; lila 20-40%; blue 40-60%; green: 60-80%; yellow 80-100%). Box plots are (bottom) strain rates along (left) and perpendicular (right) to the fibers during maximum dorsi-flexion motion without load for the individual muscle segments, with colors matching the line graphs. Note the medial compartments of the soleus (SOLla and SOLma) are only present in the more distal part of the lower leg, see Figure 2. In order to facilitate the comparison between the absolute amplitudes along and perpendicular to the fibers, the y-axis of the graph with strain rate along the fibers was inverted for the muscles expected to perform a dorsi-flexion movement. For the muscles expected to perform a plantarflexion movement, the y-axis of the graph showing strain rate perpendicular to the fibers was inverted. SOL = soleus; SOLla = lateral anterior compartment of the soleus; SOLma = medial anterior compartment of the soleus; SOLlp = lateral posterior compartment of the soleus; SOLmp = medial posterior compartment of the soleus.

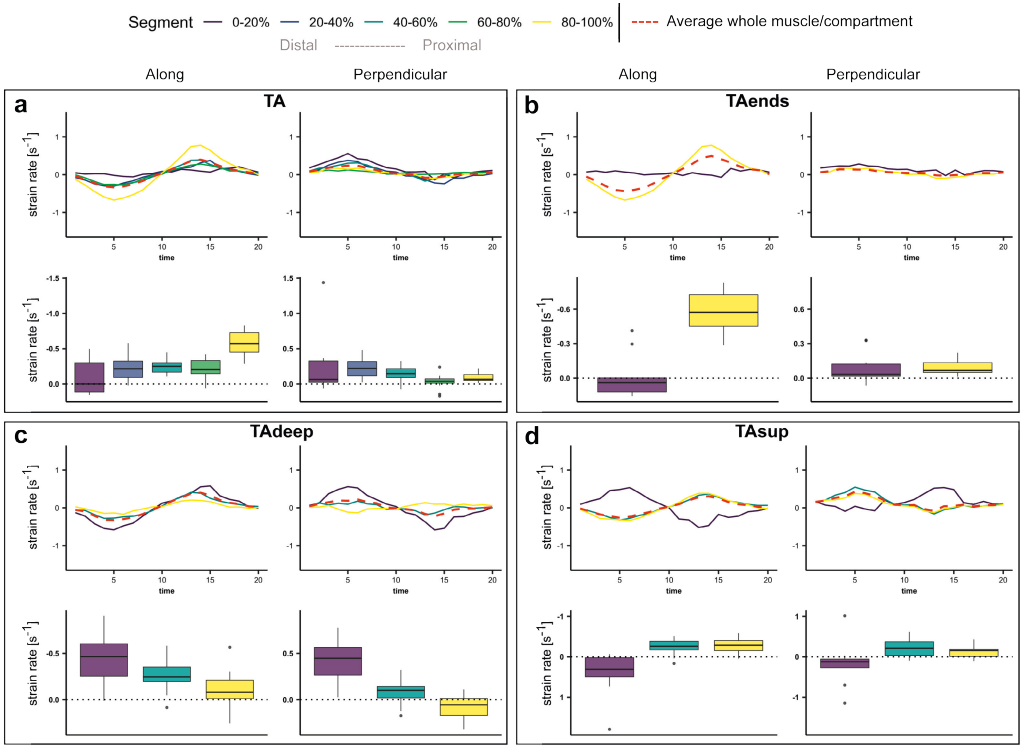

Supplemental figure 3. Line graphs (top) showing strain rate along (left) and perpendicular (right) to the fiber in the TA and the three TA compartments during the full movement cycle for the exercise with load. The strain rate pattern in the full muscle volume is depicted with a red dotted line and the 5 individual segments are depicted in different colors (purple 0-20%; lila 20-40%; blue 40-60%; green: 60-80%; yellow 80-100%). Box plots are (bottom) strain rates along (left) and perpendicular (right) to the fibers during maximum dorsi-flexion motion without load for the individual muscle segments, with colors matching the line graphs. Note not all compartments of TA muscle are continuously present along the proximodistal axis of the muscle, see Figure 2. To facilitate the comparison between the absolute amplitudes along and perpendicular to the fiber, the y-axis of the graph showing strain rate along the fibers was inverted for the muscles expected to perform a dorsi-flexion movement. For the muscles expected to perform a plantarflexion movement, the y-axis of the graph showing strain rate perpendicular to the fibers was inverted. TA = tibialis posterior; TAends = Two compartments distal and proximal of the tibialis anterior without visible intramuscular tendon; TAdeep = deep compartment of tibialis anterior; TAsup = superficial compartment of the tibialis anterior.

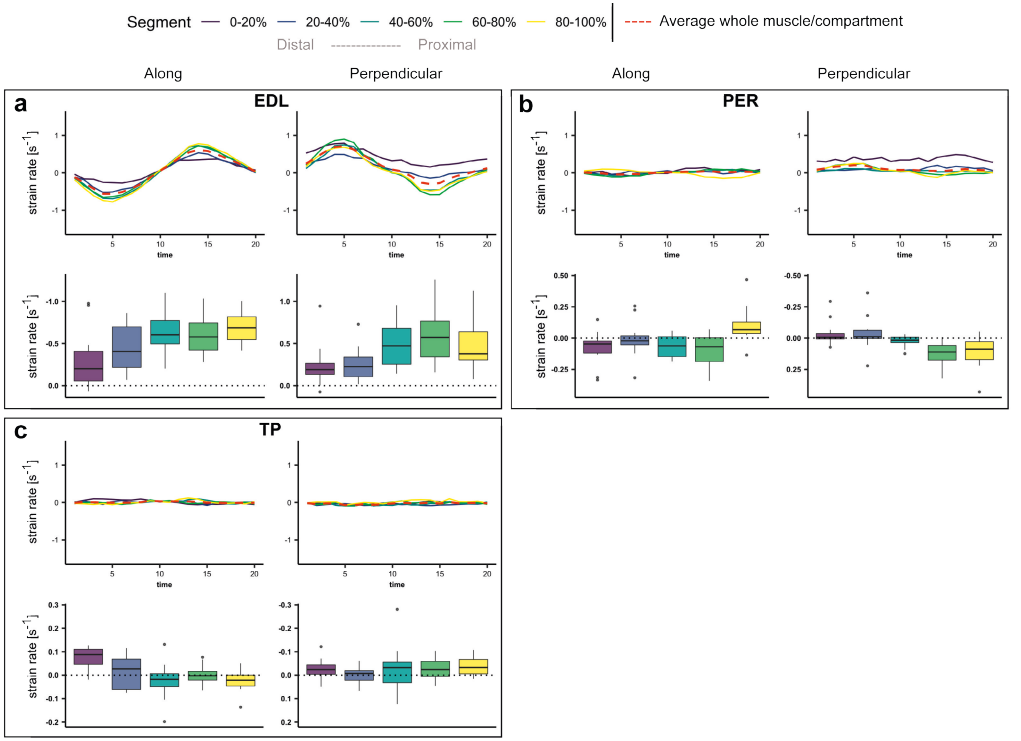

Supplemental figure 4. Line graphs (top) showing strain rate along (left) and perpendicular (right) to the fiber in the EDL, PER and TP muscle during the full movement cycle for the exercise with load. The strain rate pattern in the full muscle volume is depicted with a red dotted line and the 5 individual segments are depicted in different colors (purple 0-20%; lila 20-40%; blue 40-60%; green: 60-80%; yellow 80-100%). Box plots are (bottom) strain rates along (left) and perpendicular (right) to the fibers during maximum dorsi-flexion motion without load for the individual muscle segments, with colors matching the line graphs. In order to facilitate the comparison between the absolute amplitudes along and perpendicular to the fiber, the y-axis of the graph showing strain rate along the fiber was inverted for the muscles expected to perform a dorsi-flexion movement. For the muscles expected to perform a plantarflexion movement, the y-axis of the graph showing strain rate perpendicular to the fiber was inverted. EDL = extensor digitorum longus; PER = peroneus; TP = tibialis posterior.

REFERENCES

1. Strijkers GJ, Araujo ECA, Azzabou N, Bendahan D, Blamire A, Burakiewicz J, et al. Exploration of New Contrasts, Targets, and MR Imaging and Spectroscopy Techniques for Neuromuscular Disease - A Workshop Report of Working Group 3 of the Biomedicine and Molecular Biosciences COST Action BM1304 MYO-MRI. J Neuromuscul Dis. 2019;6(1):1-30.
2. Bodine SC, Roy RR, Meadows DA, Zernicke RF, Sacks RD, Fournier M, et al. Architectural, histochemical, and contractile characteristics of a unique biarticular muscle: the cat semitendinosus. J Neurophysiol. 1982;48(1):192-201.
3. Gans C. Fiber architecture and muscle function. Exerc Sport Sci Rev. 1982;10:160-207.
4. Lieber RL. Skeletal muscle adaptability. I: Review of basic properties. Dev Med Child Neurol. 1986;28(3):390-7.
5. Wokke BH, van den Bergen JC, Versluis MJ, Niks EH, Milles J, Webb AG, et al. Quantitative MRI and strength measurements in the assessment of muscle quality in Duchenne muscular dystrophy. Neuromuscular Disord. 2014;24(5):409-16.
6. Lokken N, Hedermann G, Thomsen C, Vissing J. Contractile properties are disrupted in Becker muscular dystrophy, but not in limb girdle type 2I. Ann Neurol. 2016;80(3):466-71.
7. Goodpaster BH, Park SW, Harris TB, Kritchevsky SB, Nevitt M, Schwartz AV, et al. The loss of skeletal muscle strength, mass, and quality in older adults: the health, aging and body composition study. J Gerontol A Biol Sci Med Sci. 2006;61(10):1059-64.
8. Englund EK, Elder CP, Xu Q, Ding Z, Damon BM. Combined diffusion and strain tensor MRI reveals a heterogeneous, planar pattern of strain development during isometric muscle contraction. Am J Physiol Regul Integr Comp Physiol. 2011;300(5):R1079-90.
9. Sinha S, Hodgson JA, Finni T, Lai AM, Grinstead J, Edgerton VR. Muscle kinematics during isometric contraction: development of phase contrast and spin tag techniques to study healthy and atrophied muscles. J Magn Reson Imaging. 2004;20(6):1008-19.
10. Zhong X, Epstein FH, Spottiswoode BS, Helm PA, Blemker SS. Imaging two-dimensional displacements and strains in skeletal muscle during joint motion by cine DENSE MR. J Biomech. 2008;41(3):532-40.
11. Drace JE, Pelc NJ. Skeletal muscle contraction: analysis with use of velocity distributions from phase-contrast MR imaging. Radiology. 1994;193(2):423-9.
12. Felton SM, Gaige TA, Reese TG, Wedeen VJ, Gilbert RJ. Mechanical basis for lingual deformation during the propulsive phase of swallowing as determined by phase-contrast magnetic resonance imaging. J Appl Physiol (1985). 2007;103(1):255-65.
13. Shin DD, Hodgson JA, Edgerton VR, Sinha S. In vivo intramuscular fascicle-aponeuroses dynamics of the human medial gastrocnemius during plantarflexion and dorsiflexion of the foot. J Appl Physiol (1985). 2009;107(4):1276-84.
14. Pamuk U, Karakuzu A, Ozturk C, Acar B, Yucesoy CA. Combined magnetic resonance and diffusion tensor imaging analyses provide a powerful tool for in vivo assessment of deformation along human muscle fibers. J Mech Behav Biomed Mater. 2016;63:207-19.

15. Fiorentino NM, Epstein FH, Blemker SS. Activation and aponeurosis morphology affect in vivo muscle tissue strains near the myotendinous junction. J Biomech. 2012;45(4):647-52.
16. Maurits NM, Bollen AE, Windhausen A, De Jager AE, Van Der Hoeven JH. Muscle ultrasound analysis: normal values and differentiation between myopathies and neuropathies. Ultrasound Med Biol. 2003;29(2):215-25.
17. Pillen S, van Alfen N. Skeletal muscle ultrasound. Neurol Res. 2011;33(10):1016-24.
18. Cunningham RJ, Loram ID. Estimation of absolute states of human skeletal muscle via standard B-mode ultrasound imaging and deep convolutional neural networks. J R Soc Interface. 2020;17(162):20190715.
19. Csapo R, Malis V, Sinha U, Sinha S. Mapping of spatial and temporal heterogeneity of plantar flexor muscle activity during isometric contraction: correlation of velocity-encoded MRI with EMG. J Appl Physiol (1985). 2015;119(5):558-68.
20. Hooijmans MT, Niks EH, Burakiewicz J, Anastasopoulos C, van den Berg SI, van Zwet E, et al. Non-uniform muscle fat replacement along the proximodistal axis in Duchenne muscular dystrophy. Neuromuscul Disord. 2017;27(5):458-64.
21. Malis V, Sinha U, Sinha S. Compressed sensing velocity encoded phase contrast imaging: Monitoring skeletal muscle kinematics. Magn Reson Med. 2020;84(1):142-56.
22. Schlaffke L, Rehmann R, Froeling M, Kley R, Tegenthoff M, Vorgerd M, et al. Diffusion tensor imaging of the human calf: Variation of inter- and intramuscle-specific diffusion parameters. J Magn Reson Imaging. 2017;46(4):1137-48.
23. Boss A, Heskamp L, Breukels V, Bains LJ, van Uden MJ, Heerschap A. Oxidative capacity varies along the length of healthy human tibialis anterior. J Physiol. 2018;596(8):1467-83.
24. Veeger TTJ, Hirschler L, Baligand C, Franklin SL, Webb AG, de Groot JH, et al. Microvascular response to exercise varies along the length of the tibialis anterior muscle. NMR Biomed. 2022;35(11):e4796.
25. Sinha U, Malis V, Csapo R, Moghadasi A, Kinugasa R, Sinha S. Age-related differences in strain rate tensor of the medial gastrocnemius muscle during passive plantarflexion and active isometric contraction using velocity encoded MR imaging: potential index of lateral force transmission. Magn Reson Med. 2015;73(5):1852-63.
26. Sinha U, Malis V, Csapo R, Narici M, Sinha S. Shear strain rate from phase contrast velocity encoded MRI: Application to study effects of aging in the medial gastrocnemius muscle. J Magn Reson Imaging. 2018;48(5):1351-7.
27. Mazzoli V, Gottwald LM, Peper ES, Froeling M, Coolen BF, Verdonschot N, et al. Accelerated 4D phase contrast MRI in skeletal muscle contraction. Magn Reson Med. 2018;80(5):1799-811.
28. Baskin RJ, Paolini PJ. Volume change and pressure development in muscle during contraction. Am J Physiol. 1967;213(4):1025-30.
29. Gottwald LM, Peper ES, Zhang Q, Coolen BF, Strijkers GJ, Nederveen AJ, et al. Pseudo-spiral sampling and compressed sensing reconstruction provides flexibility of temporal resolution in accelerated aortic 4D flow MRI: A comparison with k-t principal component analysis. NMR Biomed. 2020;33(4):e4255.
30. Klein S, Staring M, Murphy K, Viergever MA, Pluim JP. elastix: a toolbox for intensity-based medical image registration. IEEE Trans Med Imaging. 2010;29(1):196-205.
31. Yushkevich PA, Piven J, Hazlett HC, Smith RG, Ho S, Gee JC, et al. User-guided 3D active contour segmentation of anatomical structures: significantly improved efficiency and reliability. Neuroimage. 2006;31(3):1116-28.

32. Bolsterlee B, Finni T, D'Souza A, Eguchi J, Clarke EC, Herbert RD. Three-dimensional architecture of the whole human soleus muscle in vivo. PeerJ. 2018;6:e4610.
33. Pappas GP, Asakawa DS, Delp SL, Zajac FE, Drace JE. Nonuniform shortening in the biceps brachii during elbow flexion. J Appl Physiol (1985). 2002;92(6):2381-9.
34. Silder A, Reeder SB, Thelen DG. The influence of prior hamstring injury on lengthening muscle tissue mechanics. J Biomech. 2010;43(12):2254-60.
35. Malis V, Sinha U, Csapo R, Narici M, Sinha S. Relationship of changes in strain rate indices estimated from velocity-encoded MR imaging to loss of muscle force following disuse atrophy. Magn Reson Med. 2018;79(2):912-22.
36. Jensen ER, Morrow DA, Felmlee JP, Murthy NS, Kaufman KR. Characterization of three dimensional volumetric strain distribution during passive tension of the human tibialis anterior using Cine Phase Contrast MRI. J Biomech. 2016;49(14):3430-6.
37. Oda T, Himeno R, D CH, Chino K, Kurihara T, Nagayoshi T, et al. In vivo behavior of muscle fascicles and tendinous tissues in human tibialis anterior muscle during twitch contraction. J Biomech. 2007;40(14):3114-20.
38. Bojsen-Moller J, Schwartz S, Kalliokoski KK, Finni T, Magnusson SP. Intermuscular force transmission between human plantarflexor muscles in vivo. J Appl Physiol (1985). 2010;109(6):1608-18.
39. Hodgson JA, Finni T, Lai AM, Edgerton VR, Sinha S. Influence of structure on the tissue dynamics of the human soleus muscle observed in MRI studies during isometric contractions. J Morphol. 2006;267(5):584-601.
40. Adamicova K, Fetisovova Z, Malis V, Malisova S. [Bloch-Sulzberg syndrome in pathology]. Cesk Patol. 2007;43(3):109-13.
41. Blemker SS, Pinsky PM, Delp SL. A 3D model of muscle reveals the causes of nonuniform strains in the biceps brachii. J Biomech. 2005;38(4):657-65.
42. Heskamp L, Miller AR, Birkbeck MG, Hall J, Schofield IS, Blamire AM, et al. In vivo 3D imaging of human motor units in upper and lower limb muscles. Clin Neurophysiol. 2022;141:91-100.
43. Azizi E, Brainerd EL, Roberts TJ. Variable gearing in pennate muscles. Proc Natl Acad Sci U S A. 2008;105(5):1745-50.